



AFRL-RZ-WP-TP-2009-2211

**STRESS FIELD EVOLUTION IN A BALL BEARING
RACEWAY FATIGUE SPALL (PREPRINT)**

Nagaraj K. Arakere, Nathan Branch, Vaughn Svendsen, and Nelson H. Forster

**Mechanical Systems Branch
Turbine Engine Division**

OCTOBER 2009

Approved for public release; distribution unlimited.

See additional restrictions described on inside pages

STINFO COPY

**AIR FORCE RESEARCH LABORATORY
PROPULSION DIRECTORATE
WRIGHT-PATTERSON AIR FORCE BASE, OH 45433-7251
AIR FORCE MATERIEL COMMAND
UNITED STATES AIR FORCE**

REPORT DOCUMENTATION PAGE				Form Approved OMB No. 0704-0188	
<p>The public reporting burden for this collection of information is estimated to average 1 hour per response, including the time for reviewing instructions, searching existing data sources, gathering and maintaining the data needed, and completing and reviewing the collection of information. Send comments regarding this burden estimate or any other aspect of this collection of information, including suggestions for reducing this burden, to Department of Defense, Washington Headquarters Services, Directorate for Information Operations and Reports (0704-0188), 1215 Jefferson Davis Highway, Suite 1204, Arlington, VA 22202-4302. Respondents should be aware that notwithstanding any other provision of law, no person shall be subject to any penalty for failing to comply with a collection of information if it does not display a currently valid OMB control number. PLEASE DO NOT RETURN YOUR FORM TO THE ABOVE ADDRESS.</p>					
1. REPORT DATE (DD-MM-YY) October 2009		2. REPORT TYPE Journal Article Preprint		3. DATES COVERED (From - To) 01 September 2008 – 01 April 2009	
4. TITLE AND SUBTITLE STRESS FIELD EVOLUTION IN A BALL BEARING RACEWAY FATIGUE SPALL (PREPRINT)				5a. CONTRACT NUMBER In-house	
				5b. GRANT NUMBER	
				5c. PROGRAM ELEMENT NUMBER 62203F	
6. AUTHOR(S) Nathan A. Branch and Nagaraj K. Arakere, (University of Florida) Vaughn Svendsen and Nelson H. Forster (AFRL/RZTM)				5d. PROJECT NUMBER 3048	
				5e. TASK NUMBER 06	
				5f. WORK UNIT NUMBER 304806IH	
7. PERFORMING ORGANIZATION NAME(S) AND ADDRESS(ES) University of Florida Mechanical & Aerospace Engineering Gainesville, FL 32611-6300				8. PERFORMING ORGANIZATION REPORT NUMBER AFRL-RZ-WP-TP-2009-2211	
9. SPONSORING/MONITORING AGENCY NAME(S) AND ADDRESS(ES) Air Force Research Laboratory Propulsion Directorate Wright-Patterson Air Force Base, OH 45433-7251 Air Force Materiel Command United States Air Force				10. SPONSORING/MONITORING AGENCY ACRONYM(S) AFRL/RZTM	
				11. SPONSORING/MONITORING AGENCY REPORT NUMBER(S) AFRL-RZ-WP-TP-2009-2211	
12. DISTRIBUTION/AVAILABILITY STATEMENT Approved for public release; distribution unlimited.					
13. SUPPLEMENTARY NOTES Journal article submitted to the Society of Tribologists and Lubrication Engineers. PAO Case Number: 88ABW-2009-2032, 09 May 2009. Paper contains color. The U.S. Government is joint author of this work and has the right to use, modify, reproduce, release, perform, display, or disclose the work.					
14. ABSTRACT The governing mechanisms of fatigue spall propagation in ball bearing inner raceways are investigated through the use of elastic-plastic finite element modeling, X-Ray Diffraction, and the visual inspection of fatigue spall cracks. The model simulates multiple ball impacts with a fatigue spall's edge in a 208 size ball bearing operating at 10,000 rpm. Ball impacts are shown to cause severe plastic deformation within the spall edge and induce tensile residual stresses. The finite element results are supported by X-Ray Diffraction measurements and the locations of cracks observed around the edge of a spall.					
15. SUBJECT TERMS Rolling Element Bearings, Rolling Contact Fatigue, Spall Propagation, Contact Mechanics, Bearing Steels, Gas/Jet Turbines, Impact Wear, Elastic-Plastic Finite Element Analysis, Residual Stresses, X-Ray Diffraction					
16. SECURITY CLASSIFICATION OF:			17. LIMITATION OF ABSTRACT: SAR	18. NUMBER OF PAGES 44	19a. NAME OF RESPONSIBLE PERSON (Monitor) Garry D. Givan 19b. TELEPHONE NUMBER (Include Area Code) N/A
a. REPORT Unclassified	b. ABSTRACT Unclassified	c. THIS PAGE Unclassified			

Title: Stress Field Evolution in a Ball Bearing Raceway Fatigue Spall

Authors: Nathan A. Branch and Nagaraj K. Arakere¹
Mechanical & Aerospace Engineering
University of Florida
Gainesville, FL, 32611

Vaughn Svendsen and Nelson H. Forster
Propulsion Directorate
Air Force Research Laboratory
Wright Patterson Air Force Base, Ohio, 45433

Abstract

The governing mechanisms of fatigue spall propagation in ball bearing inner raceways are investigated through the use of elastic-plastic finite element modeling, X-Ray Diffraction, and the visual inspection of fatigue spall cracks. The model simulates multiple ball impacts with a fatigue spall's edge in a 208 size ball bearing operating at 10,000 rpm. Ball impacts are shown to cause severe plastic deformation within the spall edge and induce tensile residual stresses. The finite element results are supported by X-Ray Diffraction measurements and the locations of cracks observed around the edge of a spall.

Keywords

Rolling Element Bearings, Rolling Contact Fatigue, Spall Propagation, Contact Mechanics, Bearing Steels, Gas/Jet Turbines, Impact Wear, Elastic-Plastic Finite Element Analysis, Residual Stresses, X-Ray Diffraction

¹ Corresponding author, nagaraj@ufl.edu

Introduction

The ever increasing demand for safer and more efficient military and commercial jet aircraft engines has encouraged the design of high performance bearings that have better corrosion resistance, longer rolling contact fatigue (RCF) life, and higher thrust load capacity. Hybrid bearings that use silicon nitride balls and case hardened metal raceways can meet these demands and substantially out-perform conventional through-hardened steel bearings (1-3).

However, even high performance bearings are not immune from the deleterious effects caused by improper lubrication, foreign object debris (FOD), and excessive loading; all of which can cause surface fatigue failure (4). These surface fatigue failures occur in the form of surface pitting or spalls on a ball or raceway surface. This type of surface fatigue failure is also observed in gears, cam-followers, and rails (5, 6).

Conventional bearing fatigue life is usually defined as the amount of time or number of load cycles needed to initiate a surface spall. Impending bearing failure from rolling contact fatigue cannot be accurately predicted or detected until the bearing has started to liberate material in the form of fatigue spalls. Thus, the period of time from spall initiation to total failure becomes quite important. More robust materials with a high resistance to fatigue crack initiation and low spall propagation rate would help extend the period of detection and improve engine reliability.

Past and Current Research

Understanding the effects of plasticity, contact stress, fatigue, material microstructure, rate dependency, and residual stress formation in the vicinity of a spall are essential to designing safer bearings. However research of the governing mechanisms of spall propagation is limited. Probabilistic bearing life prediction models that are based on equations developed by Lundberg and Palmgren (7) are often used to estimate the life of a spalled bearing but neglect important effects such as localized plasticity. A comprehensive review and comparison of these bearing life theories is presented by Zaretsky et al (8) and Sadeghi et al (4). Kotzalas and Harris (9) studied spall progression on CVD AISI 52100 steel balls that were driven by VIM VAR M50 steel V-Ring raceways, and extended the bearing life prediction methods of Ioannides and Harris (10) to predict the remaining useful life of spalled bearings. Xu and Sadeghi (11) implemented damage accumulation laws within representative volume elements undergoing RCF to model the transformation of a dent into a progressed spall.

The spall propagation experiments on tapered roller bearings by Hoeprich (12) highlighted the randomness inherent to spall propagation and its unknown governing mechanisms. In a recent three-part series, an experimental and numerical investigation of spall propagation was presented (13-15). Part I by Rosado et al (13) showed the dependency of spall propagation rate on material selection and contact stress. Part II by Arakere et al (14) presented the static elastic-plastic stress fields around an initial fatigue spall, the likely conditions that contribute to initial spall growth, and the importance of including plasticity effects in bearing fatigue life calculations. Part III by Forster et al (15) investigated the effects of alloy content, heat treatment, and residual stresses on the

stability of the microstructure and alterations in residual stress profile ultimately impacting bearing fatigue life and propagation rate.

The analysis presented here is unique because it uses finite element models that include the effects of plasticity to calculate the critical stresses and strains that develop within a spall edge during and after successive ball impacts. The results are supported by the residual stresses calculated by X-Ray Diffraction techniques and the location of cracks on an impacted spall edge. This information will support a plausible scenario of why fatigue spalls propagate. This analysis represents a first step toward identifying how material properties, bearing geometry, and operating conditions contribute to spall propagation and eventual bearing failure.

Nature of Spall Propagation

Spalls propagate predominately in the direction of ball motion during surface fatigue failure in bearings (12, 13). Figure 1 shows an example of damage progression along a bearing inner raceway. In the experiments explained in (13), spalls are initiated naturally from material fatigue or by Rockwell C indentations which act as stress risers and accelerate the spall initiation process. During bearing operation cracks develop around the indent, liberate surface material, and form a small initial spall. The initial spall will widen during operation as described in (14) and eventually allow the ball to descend into the spall and impact the trailing edge. The spall will then progress around the raceway in the direction of ball motion until catastrophic failure occurs (fig 1.c). Usually the catastrophic failure mode is fracture of the bearing cage leading to bearing seizure.

The spall's trailing edge will be defined as the edge that deteriorates with continuous bearing operation, whereas the spall's leading edge is a portion of the initial spall and does not liberate significant material during operation.

The numerous impacts that occur between balls and the trailing edge of the spall are believed to be the main driving forces of spall propagation (fig 2). The trailing edge is the only spall edge that is subjected to ball impacts *and* deteriorating: clearly there is a relationship between the two.

Also, significant cracks form only on the spall's trailing edge (figs 3 & 4) as the spall is propagating. This is another indication that more damage is occurring on the impacted edge in the form of cracks and not on the leading edge. Continuous ball impacts are believed to encourage these edge cracks to grow and cause fragments of

material to liberate from the raceway's surface. The fragments collected by the Oil Debris Monitor in (13) were typically the same size as the edge of the spall.

This continuous loss of surface material increases the clearance between the bearing's inner and outer raceways which creates enough space for the engine shaft to misalign. Severe vibrations, heat, noise, and eventual catastrophic bearing failure are then likely to occur.

Procedure and Finite Element Model

The finite element model must capture the geometry and physics of bearing operation as accurately as possible. However, this analysis will not model the entire inner and outer rings, all balls, lubrication, temperature effects, and interactions with the bearing cage. For this purpose, only a segment of the inner ring will be modeled in the interest of computational efficiency (fig 5). The raceway segment will include the trailing edge of the spall since we are investigating the types of damage this specific spall edge is likely to develop during ball impact.

To best capture the geometry of the spall's edge, profilometer tracings were taken of the spall's trailing edge on four different raceways made of Pyrowear 675 (P675) case hardened and M50 through-hardened bearing steels (fig 6.a). An average spall edge slope of 45 degrees is determined from the four profile measurements and is applied to the FE model geometry (fig 6.b). This edge geometry is constant during spall propagation (fig 6.b), and suggests that the failure mode controlling material loss from the spall's edge is the same regardless of spall length.

The finite element model will simulate three successive rigid ball impacts on the same spall edge at a ball velocity of 15.24 m/s (50 ft/s) (fig 7). The ball velocity is determined from the known rotational speeds of the cage and inner raceway of the 40 mm bearing used in (13-15). Three impacts were chosen because there was no significant change in the stresses and strains within the spall edge after the second and third impacts.

Rigid balls do not require a mesh and reduce the number of elements in the model. All three of the balls have the density of steel (8 g/cm^3) and are expected to impart more energy into the spall than compared to a silicon nitride ball. The ball is not

allowed to spin and can only translate within the plane of symmetry. Since contact is frictionless, the rotational kinetic energy of the ball will not significantly affect the nature of impact between ball and spall edge.

In house compression tests were performed on M50 steel specimens (fig 8) to obtain its stress strain curve up to 0.013 plastic strain and compared well with data available from Carpenter (16). Since the plastic behavior of this material after 1.3% plastic strain is unknown or unobtainable from other sources, the material is assumed to behave in a perfectly plastic manner after this strain is reached. Typically, very hard materials do not have a capacity to strain harden like copper or 303 stainless steel, so a perfectly plastic response is a reasonable assumption for this bearing steel and this analysis.

A very fine linear hexahedral mesh is designed around the spall's edge because the most critical stresses and strains are forming within this small region (fig 7). The Explicit solver within ABAQUS v6.8-2 was used since this is a transient analysis and has time dependent properties (the velocity of the ball) (17). The von Mises (J2) failure criterion, associative flow rule, and isotropic hardening are appropriate for bearing steels and implemented here.

Results and Discussion

All plots of the finite element model results will be close up images of a spall edge's cross section (fig 9). The radial and hoop stresses within the spall *during* impact were calculated (fig 9) and are mostly compressive as expected. The maximum contact pressure between a ball and spall edge can reach 7 GPa which is sufficient to cause subsurface yielding. Classical Hertzian contact solutions do not apply here since the spall edge is very sharp and is undergoing considerable deformation during impact.

Of greater interest are the locations and distributions of *residual* tensile stresses around the edge of the spall. It is well understood that tensile residual stresses are detrimental to the fatigue strength of a material because they encourage fatigue crack initiation and growth. The finite element model calculates tensile residual hoop stresses to occur on the surface of the spall's edge after successive ball impacts (fig 10). This is significant because this location of residual tensile stress agrees with where cracks are seen around the spall's edge in the bearings from (13, 15) (figs 3 & 4).

The locations and magnitudes of residual hoop stresses within the spall's edge from the FE results are shown in figures 10 and 11. Locations D and E best capture the residual tensile stress at the surface mentioned earlier and the residual compressive stresses just beneath the spall's edge. The severity of the residual stresses decreases going away from the spall's edge as shown in profiles A, B, and C.

Also, locations A, B, and C of the finite elements results match closely to the profiles calculated from X-ray diffraction (XRD) techniques (fig 12) and described in more detail in (15). The results of Forster et al (15) showed that the changes in residual stress were cumulative over millions of cycles in AISI 52100, AISI M50 and M50 NiL

bearings. XRD was done on bearing raceways that had experienced 10^6 to 10^{10} stress cycles whereas the model is only simulating three impacts. Therefore, only qualitative comparisons can be made here.

For example, the residual stress profile in figure 12.a (15) is from a spall initiated from surface indents and is quite different from the spall initiated from material fatigue without surface indents (fig 12.b). This is not captured in the bearing model, and may be a result of microstructure decay (15). Also, the location of the experimental XRD measurement was about 3.2 mm (0.125 inches) from the edge of the spall in all cases. The spot size of the irradiated area is 1.3 mm x 1.3 mm.

The XRD residual stress profiles are not a close match to profiles D and E because the location where XRD was performed was not close enough to the spall's edge to measure the residual tensile stresses shown in profiles D and E. Even if XRD was taken on locations D and E, unknown cracks within the spall's edge could have relieved residual stresses that XRD could not have picked up. This helps explain why the data is not an exact match for every location, but profiles A, B, and C are within the ballpark of what is determined from XRD.

Many fatigue failure theories predict tensile *radial* residual stresses to develop in rolling contact (4) which lead to crack formation parallel to the surface. The finite element results show that tensile radial residual stresses exist within the edge of the spall after successive impacts (fig 13).

Radial tensile residual stresses encourage fatigue cracks to form and their location matches the spall depth (figs 13 & 2). Residual stress profiles are plotted (fig 14) at the same locations as the hoop direction plot (fig 10). Locations D and E capture the residual

compressive stresses just below the spall's edge, while B and C show subsurface residual tensile radial stresses at the same depth as the depth of the spall. The location of residual tensile radial stress explains why the spall depth is consistent throughout spall growth.

The finite element results in figures 10 and 13 show compressive residual stresses in both the radial and hoop directions located just below the spall's edge. Compressive residual stresses below the spall's edge retard crack growth (18), and consequently keep material loss localized to the immediate surface. This is observed in experiments and shown in figures 2, 3 and 4.

The location of residual tensile hydrostatic pressure also agrees with where cracks appear in spalled bearings (figs 15 & 3). ABAQUS defines tensile hydrostatic pressure as negative, which is why the tensile region is blue instead of red as before. Howell et al (19) studied rolling contact over a surface indent and showed that cracks are likely to initiate in regions of tensile hydrostatic pressure.

The strain life approaches summarized in (18), such as Coffin-Manson, have shown that fatigue cracks are likely to initiate in a region of high plastic strain over many load cycles. A detailed quantitative fatigue life analysis cannot be made here since the cyclic strain-life data for bearing steels is scarce, the plastic strains calculated by the FE model are for a spall that has only suffered three impacts, and the cyclic plastic strain amplitudes from the FE model are highly dependent on the cyclic hardening law which is also limited for bearing steels. However, as a qualitative investigation it is worth comparing the distribution of plastic strain within the spall edge with the location of cracks in the actual bearings to see if cracks form in the most damaged region as predicted by the FE model.

Large amounts of plastic strain in the hoop direction develop on the surface of the spall's edge (figure 16) and match closely to where cracks are observed in actual bearing spalls (figs 3 & 4). The maximum hoop plastic strain is below the surface and is a likely site of crack initiation.

The distribution of maximum principal plastic strain (fig 17) corresponds to the locations of residual tensile hoop stress (fig 10), residual radial tensile stress (fig 13), residual tensile hydrostatic pressure (fig 15), and hoop plastic strain (fig16). Cracks are likely to follow this path of highly damaged material and also aided by the tensile and compressive residual stresses within the spall.

To verify the assumption that cracks follow the path of maximum principal plastic strain, it is shown that the distribution of maximum principal plastic strain (fig 17) is also similar to the profilometer tracings of the spall edges (fig 6). After a fragment of material is liberated from the spall edge, the new spall edge profile left behind is a close match to the profilometer tracings *and* the distribution of maximum principal plastic strain. This process repeats itself and explains why the spall edge profile does not vary throughout spall propagation.

Spall edge geometry is expected to influence the calculation of stresses and strains in the finite element model; however it can be shown that similar residual stress gradients will develop regardless of spall edge sharpness (figs 18 & 19). Two different degrees of spall sharpness were modeled with the same ball velocity and material properties as before. Stress contours of the residual radial stresses within the spall's edge are shown along with a graph of the residual hoop stress profiles. As expected, the stresses around a

blunt spall are not as severe as the sharper spall edge, but the fact that the stress gradients are similar helps show the dependency of spall shape in the finite element results.

Conclusions

This analysis represents a first attempt to capture the critical stresses and strains that develop in a spall edge during and after successive ball impacts. The validity of the finite element results is strengthened by the locations and magnitudes of the residual stress profiles calculated from XRD techniques and the locations of cracks on the impacted spall edges observed in spall propagation experiments.

It is well understood that residual tensile stresses decrease the fatigue life of a material (4). The finite element model determines residual hoop, radial, and hydrostatic tensile stresses to occur within an impacted spall edge at the same locations where fatigue cracks are observed in experiments. The computed residual compressive stresses below the trailing edge of the spall retard crack growth and keep material loss localized to the immediate surface as seen in experiments.

The distribution of plastic strain within the spall edge provides a likely path of crack growth which leads to the liberation of material fragments during spall propagation. This is supported by the observation that the spall edge shape remains consistent throughout propagation and closely matches the distribution of maximum principal plastic strain. Qualitative strain-life methodologies predict cracks to initiate in regions of high plastic strain. Cracks appear on spall edges where the finite element model predicts large plastic strain.

Future research will investigate how the impact between the ball and spall edge is affected by the presence of the outer raceway and bearing cage. Changes in material properties due to microstructure decay are expected to occur in actual bearings and this

influence should be included. Future work will also explain why spall propagation rates differ between case and through hardened bearing materials.

Acknowledgements

This work was supported by the Air Force Research Laboratory (AFRL), Wright Patterson Air Force Base, Ohio, 45433, and the Timken Company, Canton, OH. The authors would like to thank Hitesh Trivedi of UES for taking profile measurements of the spall's trailing edges. Thanks also to Kevin Thompson of AFRL for all of the photographs of the bearing spalls and involvement in the spall propagation experiments. Sincere appreciation is expressed to Mike Klecka and Dr. Ghatu Subhash for the compression tests of the M50 steel specimens. Special thanks to Dr. Liz Cooke, Dr. Bill Hannon, and Bob Wolfe of Timken Co. for their insight and contributions to this project.

References

- (1) Miner, J. R., Dell, J., Galbato, A., and Ragen, M. A., (1996), "F-117-PW-100 hybrid bearing ceramic technology insertion," *ASME J of Engineering for Gas Turbines and Power*, V 118, pp. 434-442.
- (2) Tanimoto, K., Kajihara, K., and Yanai, K., (2000), "Hybrid ceramic ball bearings for turbochargers," *SAE Paper* 2000-01-1339, pp. 1-14.
- (3) Wang, L., Snidle, R. W., and Gu, L., (2000), "Rolling contact silicon nitride bearing technology: A review of recent research," *Wear*, Vol. 246, pp. 159-173.
- (4) Sadeghi, F., Jalalahmadi, B., Slack, T. S., Raje, N., Arakere, N. K., "A Review of Rolling Contact Fatigue," being reviewed for publication in the *ASME Journal of Tribology*.
- (5) Clarke, T.M., (1984) "The Role of Near Surface Inclusions in the Pitting of Gears," *ASLE Transactions*, Vol. 28, 1, p. 111-116.
- (6) Ringsberg, Jonas W. (2001), "Life Prediction of rolling contact fatigue crack initiation," *International Journal of Fatigue*, 23, p. 575-586.
- (7) Lundberg, G., and Palmgren, A., (1947) "Dynamic Capacity of Rolling Bearings," *Acta Polytechnica*, 1, 3, Stockholm.
- (8) Zaretsky, Erwin V., (1996), "Comparison of Life Theories for Rolling Element Bearings," *Tribology Transactions*, 39, 2, 237-248.
- (9) Kotzalas, M., Harris, T.A. (2001), Fatigue Failure Progression in Ball Bearings, *Trans. ASME*. Vol 123, 238-242.
- (10) Ioannides, E., and Harris, T., (1985), "A New Fatigue Life Model for Rolling Bearings," *ASME Journal of Tribology*, 107, 367-378.
- (11) Xu, G., Sadeghi, F. (1996), Spall initiation and propagation due to debris denting, *Wear* 201, 106-116.
- (12) Hoeprich, M.R., (1992), "Rolling Element Bearing Fatigue Damage Propagation," *ASME Journal of Tribology*, 114, April, 328-333.
- (13) Rosado, L., Forster, N., Thomson, K., "On the Rolling Contact Fatigue Life and Spall Propagation Characteristics of M50, M50 NiL and 52100 Bearing Materials: Part I - Experimental Results," being reviewed for publication in the *STLE Tribology Transactions*.
- (14) Arakere, N. K., Branch, N., Levesque, G., Svendsen, V., Forster, N.H., "On the Rolling Contact Fatigue Life and Spall Propagation Characteristics of M50, M50 NiL and 52100 Bearing Materials: Part II – Stress Modeling," being reviewed for publication in the *STLE Tribology Transactions*.
- (15) Forster, N.H., Ogden, W.P., Trivedi, H.K., "On the Rolling Contact Fatigue Life and Spall Propagation Characteristics of M50, M50 NiL and 52100 Bearing Materials: Part III - Metallurgical Examination," being reviewed for publication in the *STLE Tribology Transactions*.
- (16) Carpenter. www.carttech.com. September 15, 2009. "Hot Tensile Properties of Carpenter VIM VAR M50 Bearing Steel"
- (17) ABAQUS v6.8.2 Users Manual
- (18) Suresh, S., Fatigue of Materials. Second Edition, 2004, Cambridge University Press

- (19) Howell, M.B., Rubin, C.A., Hahn, G.T., (2004) “The Effect of Dent Size on the Pressure Distribution and Failure Location in Dry Point Frictionless Rolling Contacts,” *ASME Journal of Tribology*, July 2004, Vol 126, 413-421.

List of Figures

Figure 1. a. Virgin Raceway, b. Small Spall, c. Progressed Spall

Figure 2. Ball impact with spall's edge influences propagation direction

Figure 3. Two examples of cracks on trailing edge of propagating spall

Figure 4. Two examples of close up images of spall's edge cracks

Figure 5. Finite Element Model Geometry

Figure 6. a. Tracings of spall edges from M50 and Pyrowear 675 bearing steels, b.

Consistent spall edge during propagation and used in FE model

Figure 7. FE model of ball impacting spall edge and finite element mesh

Figure 8. Flow curve, M50 steel

Figure 9. Radial and Hoop stresses during impact

Figure 10. a. Residual stress profile in Hoop direction after 3 impacts, b. Locations of profiles in Figure 11

Figure 11. Residual hoop stress profiles, Finite element results

Figure 12. X-Ray Diffraction residual hoop stress profiles; M50 spalled bearings

Figure 13. Residual stress state in the radial direction and locations of stress profiles shown in figure 10.

Figure 14. Finite element residual stress profiles in radial direction

Figure 15. Residual hydrostatic stresses

Figure 16. Hoop and Radial plastic strain. Radial plastic strain is mostly compressive around edge of spall. Locations of large tensile hoop plastic strain is close to where cracks appear

Figure 17. Maximum principal plastic strain

Figure 18. Residual hoop stresses for blunt spall, similar to sharp spall

Figure 19. Before and after images of sharp and blunt spall. Similar radial residual stresses are obtained

Figures

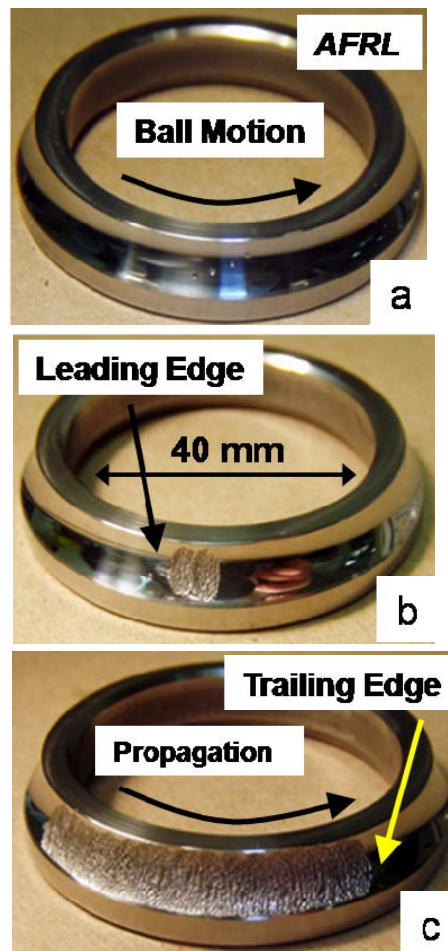


Figure 1. a. Virgin Raceway, b. Small Spall, c. Progressed Spall

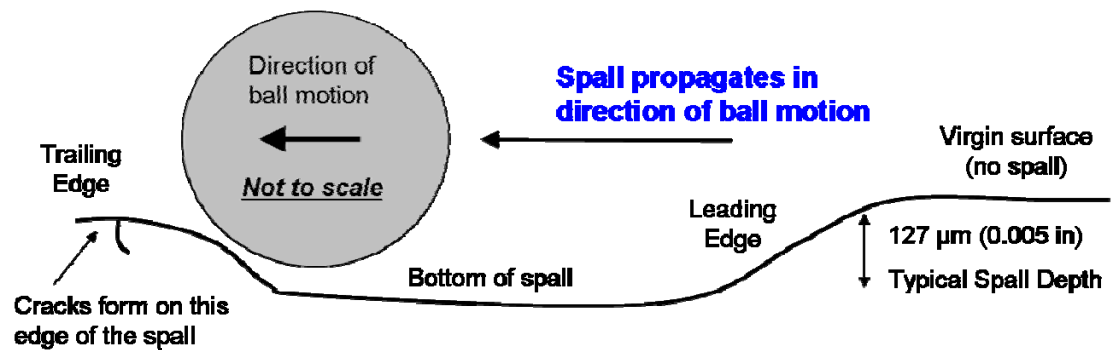


Figure 2. Ball impact with spall's edge influences propagation direction

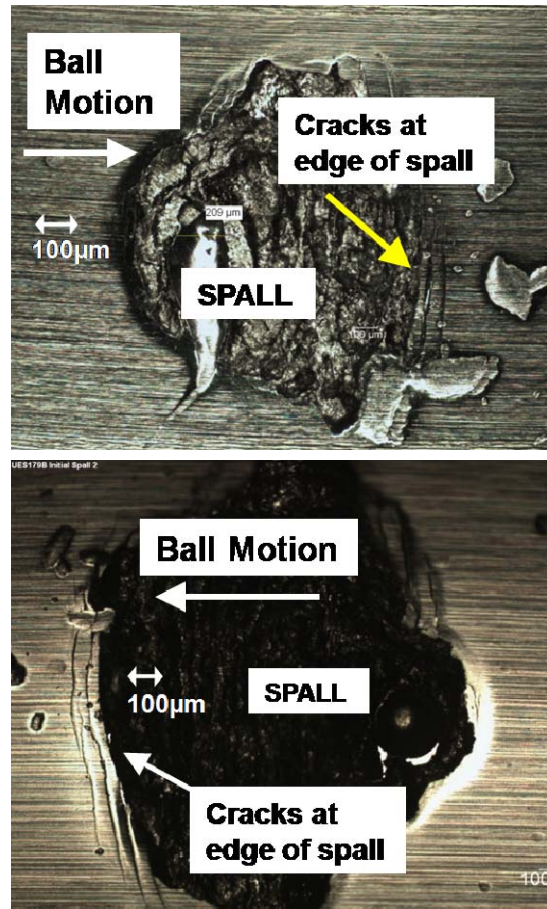


Figure 3. Two examples of cracks on trailing edge of propagating spall

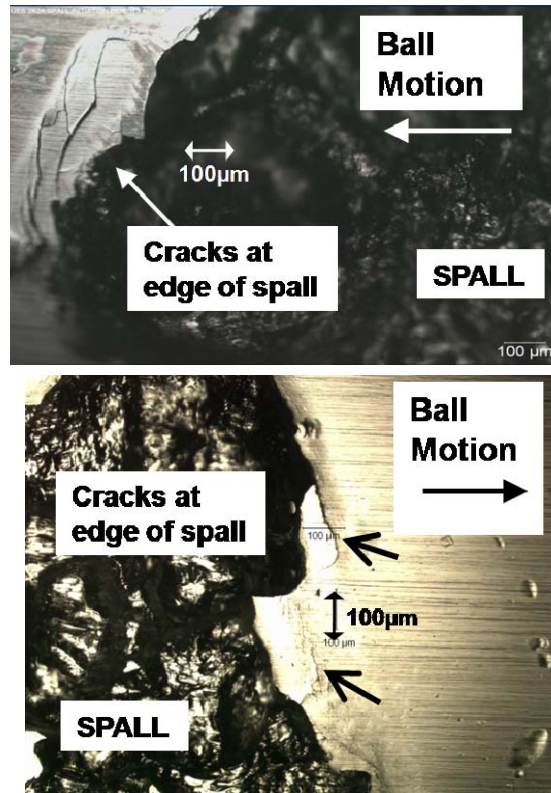


Figure 4. Two examples of close up images of spall's edge cracks

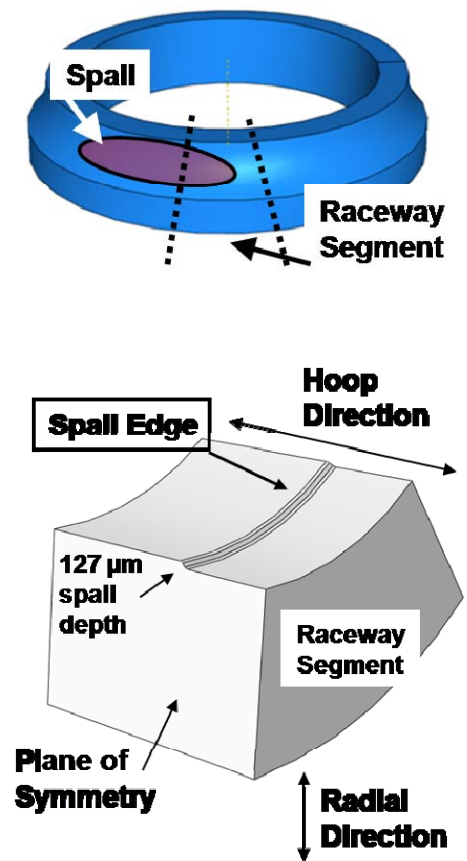


Figure 5. Finite Element Model Geometry

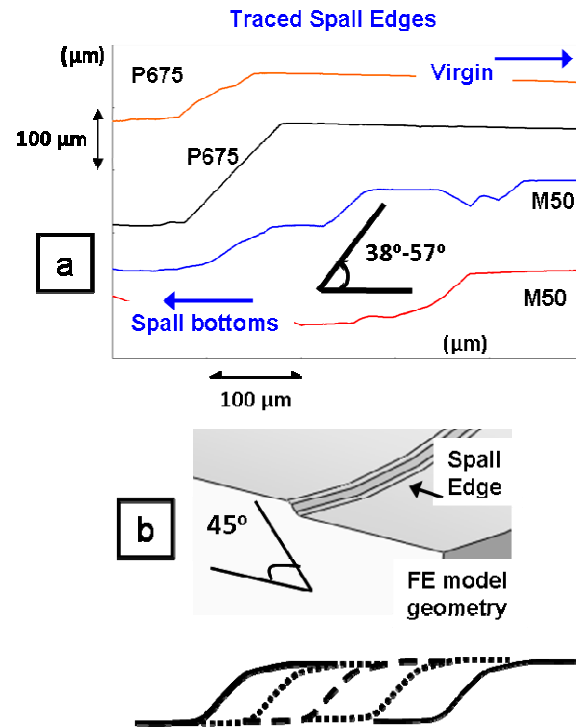


Figure 6. a. Tracings of spall edges from M50 and Pyrowear 675 bearing steels, b.

Consistent spall edge during propagation and used in FE model

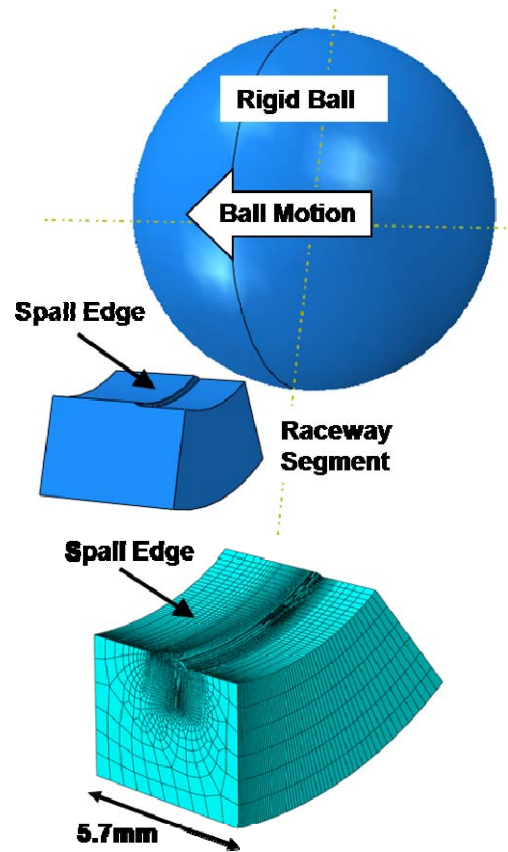


Figure 7. FE model of ball impacting spall edge and finite element mesh

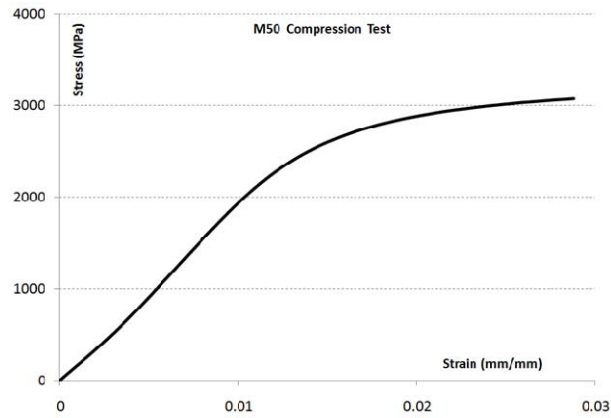


Figure 8. Flow curve, M50 steel

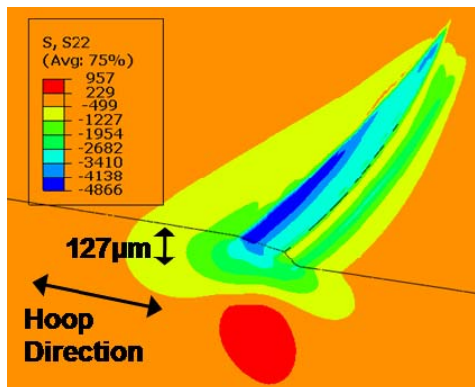
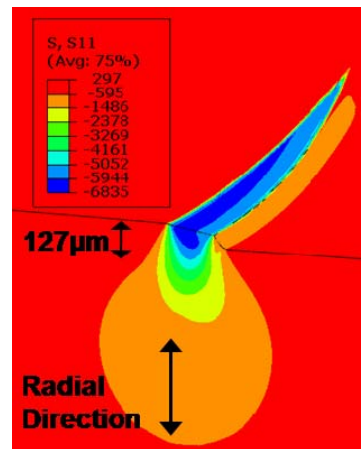
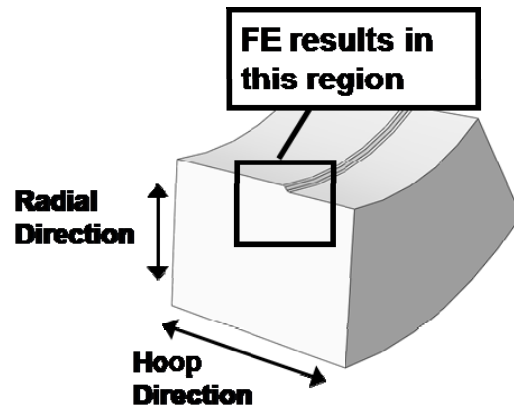


Figure 9. Radial and Hoop stresses during impact

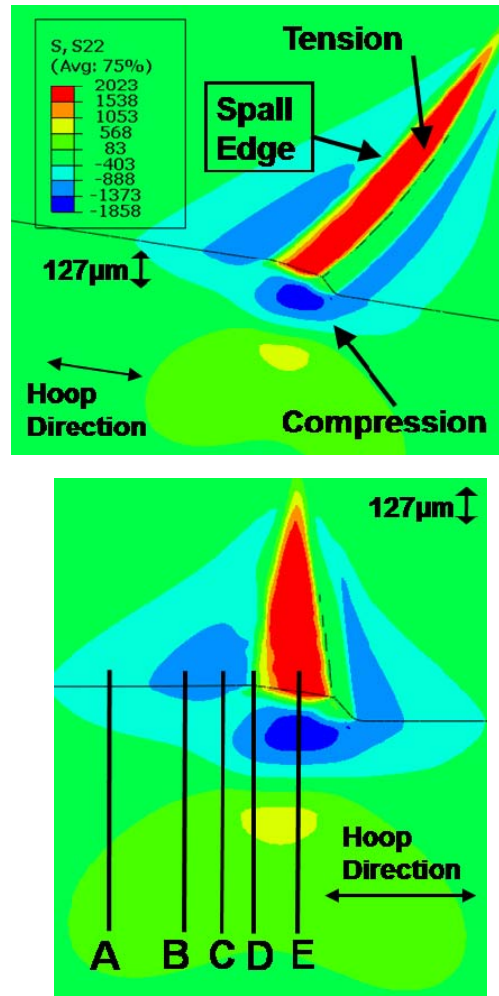


Figure 10. Residual stress profile in Hoop direction after 3 impacts and locations of profiles in Figure 11

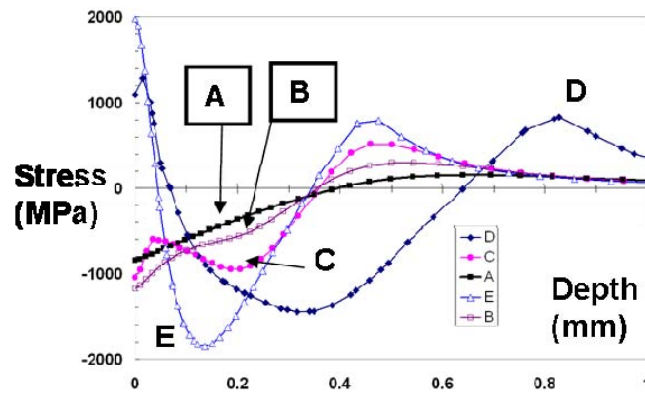
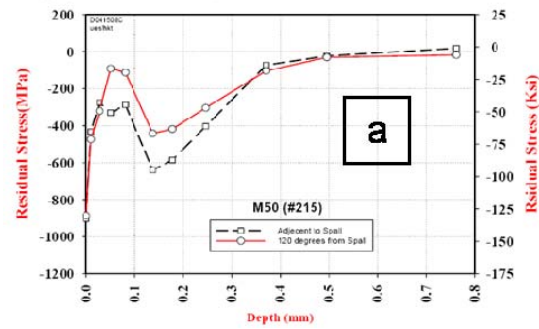


Figure 11. Residual hoop stress profiles, Finite element results

- Bearing 215 – Life tested, suspended at
- Suspended 16,343 X 10⁶ cycles at 3.01 GPa
- Propagation 31.0 X 10⁶ cycles at 2.41 GPa



- Bearing 075 - Propagation initiated on new bearing from indents
- Initiation 19.6 X 10⁶ cycles at GPa
- Propagation 187.3 X 10⁶ cycles at 2.41 GPa

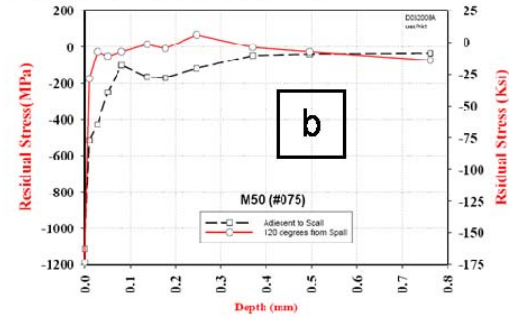


Figure 12. X-Ray Diffraction residual hoop stress profiles; M50 spalled bearings

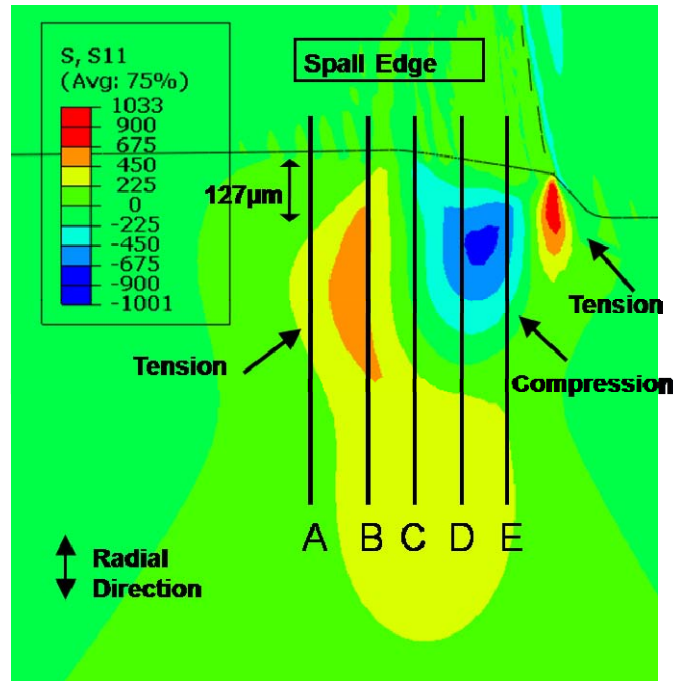


Figure 13. Residual stress state in the radial direction and locations of stress profiles shown in figure 10.

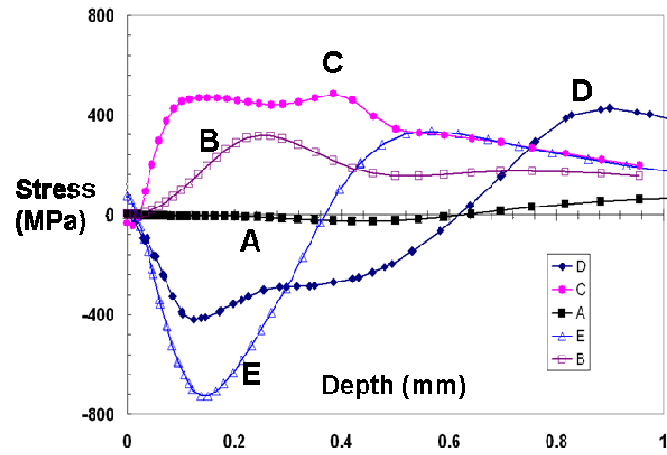


Figure 14. Finite element residual stress profiles in radial direction

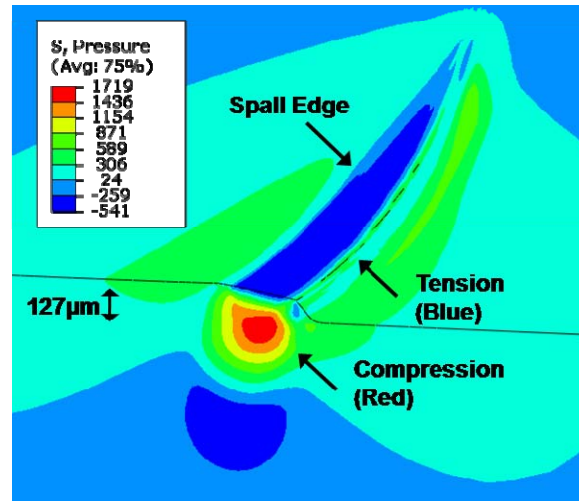


Figure 15. Residual hydrostatic stresses

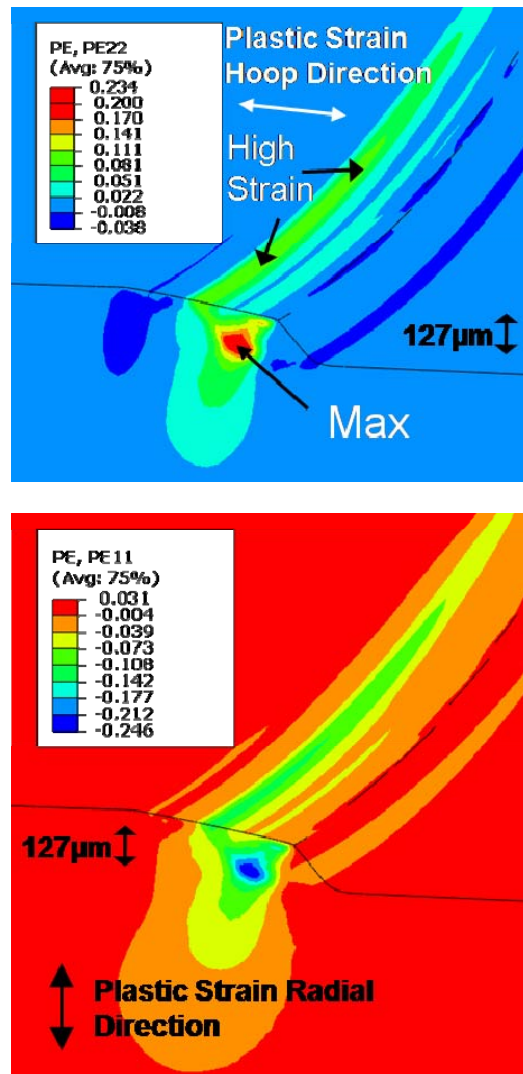


Figure 16. Hoop and Radial plastic strain. Radial plastic strain is mostly compressive around edge of spall. Locations of large tensile hoop plastic strain is close to where cracks appear

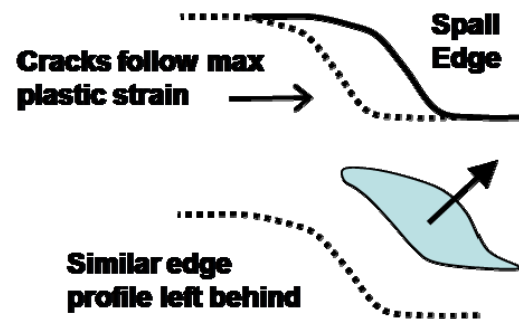
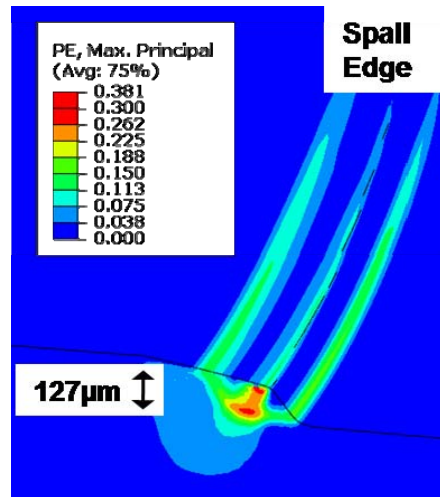


Figure 17. Maximum principal plastic strain

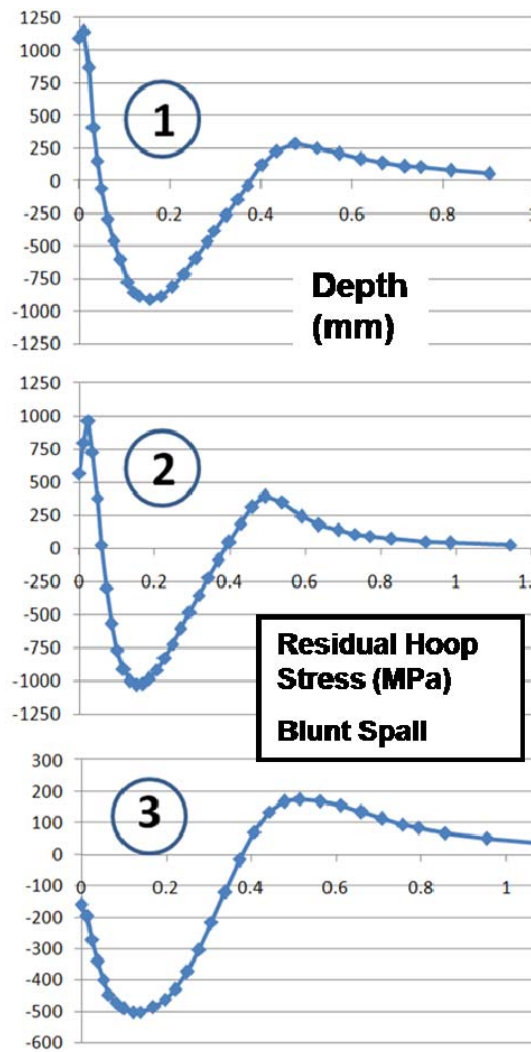
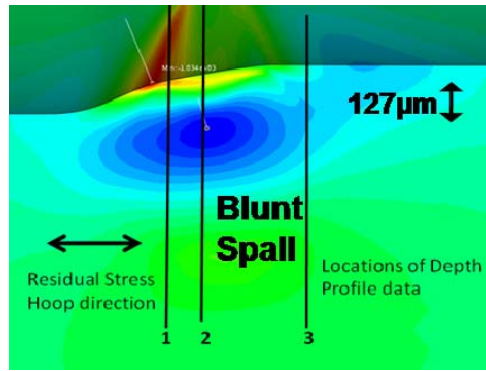


Figure 18. Residual hoop stresses for blunt spall, similar to sharp spall

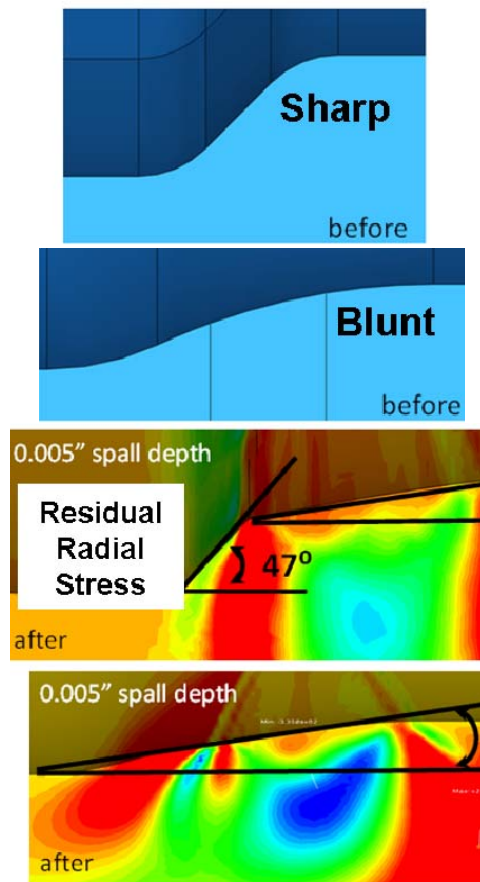


Figure 19. Before and after images of sharp and blunt spall. Similar radial residual stresses are obtained.